Synthesizing Wider WiFi Bandwidth for Respiration Rate Monitoring in Dynamic Environments

Shuyu Shi[1], Yaxiong Xie[2], Mo Li[2], Alex X. Liu[1,3] and Jun Zhao[2]
[1]State Key Laboratory for Novel Software Technology, Nanjing University, Nanjing, Jiangsu, China
[2]School of Computer Science and Engineering, Nanyang Technological University (NTU), Singapore
[3]Dept. of Computer Science and Engineering, Michigan State University, USA
ssy@nju.edu.cn, alexliu@cse.msu.edu, {limo, yxie005, junzhao}@ntu.edu.sg

***Abstract*—Respiration rate monitoring is beneficial for the diagnosis of a variety of diseases, such as heart failure and sleep disorders. Radio Frequency (RF) based respiration rate monitoring systems, namely ultra-wideband radar and COTS device, have been proposed without requiring any direct contact with the detected person. However, existing RF based systems either require expensive UWB radio (radar based) or work only in stationary environments (COTS device based). To address the limitations of both radar based and COTS device based systems, in this paper, we propose *RespiRadio*, a system that can detect a person's respiration rate in dynamic ambient environments via a single TX-RX pair of WiFi cards. The key novelty of *RespiRadio* is that it overcomes the limit of existing COTS device based respiration rate systems by synthesizing a wider-bandwidth WiFi radio. With the synthesized WiFi radio, we can identify the path reflected by the breathing person and then analyze the periodicity of the signal power measurements only from this path to infer the respiration rate. We experimentally evaluate the performance of *RespiRadio* in non-static indoor environments and the results demonstrate that the overall estimation error is 0.152 breaths per minute (bpm).**

I. Introduction

Respiration rate is a vital sign that contains valuable information for the diagnosis of diseases such as pulmonary disease [8], heart failure [14], anxiety disorders [37], and sleep disorders [10]. Some chronic diseases, such as obstructive sleep apnea syndrome (OSAS) and chronic obstructive pulmonary disease (COPD), require continuous monitoring of patient's respiration rate. Traditional approaches to the continuous monitoring in home settings use belts or garment instrumented with capacitive sensors [20], smart cushion with air pressure sensors [22], or camera based solutions [39]. Wearable device based systems have two key limitations. First, they are expensive to deploy as they require customized hardware. Second, they are inconvenient to use as they require patients to wear sensors all the time. Camera based systems have three key limitations. First, they cause privacy concerns. Second, they cannot work in dark. Third, they cannot work when the target patient is out of the sight.

To address these limitations, recently, Radio Frequency (RF) based respiration rate monitoring approaches have been proposed [6], [15], [17], [23]–[25], [32]. Such RF based approaches fall into two categories: ultra-wideband (UWB) radar based and narrowband commodity Off-The-Shelf (COTS) device based. UWB radar based monitoring systems infer the respiration rate of a human subject based on the signal variations in the propagation path reflected by the respiration person. COTS device based monitoring systems use either 802.15.4 transceivers or WiFi devices. Patwari *et al.* used tens of 802.15.4 transceivers for achieving non-contact respiration rate monitoring [23], and Kaltiokallio *et al.* further reduced the number of transceivers to two [15]. Moreover, Liu *et al.* analyzed the average peak interval of WiFi CSI measurements to detect the respiration rate of a human subject [17].

For UWB radar based respiration rate monitoring systems, the advantage is that they can achieve high precision in the presence of ambient environmental noise, but the limitation is that they require dedicated RF frontend, which is expensive [6], [24], [25], [31]. In contrast, for COTS RF device based respiration rate monitoring systems, the advantage is that they are cheap and easy to deploy, but the limitation is that the surrounding environment needs to be stationary so that respiration is the sole source of motion, because of the narrow bandwidth of COTS RF devices. We now explain why the narrow bandwidth limits existing COTS RF device based solutions to stationary environments. Given the *multipath* effect, the spatial resolution of two distinct propagation paths is determined by the *bandwidth* of the radio frequency f, which is equal to $\frac{1}{f} \cdot c$ m (c is the speed of light). Consider the scenario, where the radio is reflected by two subjects, namely human subject 1 and 2, with a distance of Δd. If we utilize a TX-RX pair of RF radio nodes with a bandwidth Δf that is smaller than $\frac{c}{\Delta d}$ Hz, the received signals reflected by the two subjects are superimposed. Assume that we are interested in monitoring the respiration rate of human Subject 1, the dynamic disturbance of human subject 2, such as walking or continuously posture changes, poses a much larger variation on the superimposed received signals, resulting in the failure of inferring the respiration rate of human subject 1.

In this paper, we present *RespiRadio*, a COTS WiFi based respiration rate monitoring system that works in dynamic environments. The insight is that WiFi devices can work on multiple frequency bands, so that we can span a much wider spectrum bandwidth than that of a single channel simply using COTS WiFi cards. Based on this insight, our idea is to transmit packets on multiple WiFi bands and exploit the aggregated CSI measurements from these different WiFi channels to synthesize a much wider-band WiFi radio. For instance, with our scheme, we can synthesize a 100 MHz WiFi radio by hopping on to five distinct WiFi channels with

a bandwidth of 20 MHz to collect channel state information (CSI) measurements. Therefore, such synthesized wideband WiFi CSI measurements can break the existing bandwidth limit of COTS WiFi interfaces while preserving the low cost compared with Radar based systems, which require expensive customized wideband RF hardware. With the synthesized much wider-bandwidth WiFi radio signals, we isolate the signal path reflected by breathing human from other paths impacted by other obstacles and then analyze the periodicity of the signal power measurements only from the breathing-affected path to estimate the respiration rate. Therefore, compared with existing COTS based systems, *RespiRadio* can estimate respiration rate of a human subject more accurately in dynamic indoor environments.

In this paper, we address the following four challenges: fast channel switching, respiration person isolation, non-respiration variation removal and respiration rate estimation.

Fast Channel Switching: We need to collect CSI measurements from multiple WiFi channels to synthesize a wider-band WiFi radio within the coherence time, as they are else uncorrelated, and hence invalid for channel synthesization. Default channel switching mechanism in 802.11 protocol consumes at least several seconds, which is far beyond the system requirement. Also, our system runs on existing WiFi APs so that channel switching requires not to interfere with normal 802.11 client-AP association and normal networking services. To address the challenges, we modify re-association method in 802.11 protocol to leverage regular 802.11 beacon frames for synchronous, protocol compliant channel switching, achieving a low latency of 15 ms.

Respiration Person Isolation: As respiration monitoring relies upon the reflection path of the testee to detect their respiration rate; however, the distance between the testee and the TX-RX WiFi pair is unknown, that means that the correct signal path reflected from the testee must be identified. We propose to detect the periodicity of the amplitude fluctuation on the path conditioned on the repeated expanding and contraction of the testee's chest cavity.

Non-respiration Variation Removal: Even after identifying the signal path, it is still challenging to remove non-respiration related channel variations, as erratic motions like posture change or limb swing also induce variations to the signal path that represents the respiration-related fluctuation. Such motions often dominate the path variations, which leads to significant changes to the signal measurements and thus reduces the recognition accuracy. We propose a two-state hidden Markov model (HMM) to differentiate motions due to respiration from other motion.

Respiration Rate Estimation: As we aim to monitor respiration rate *continuously*, it is of vital importance to design an estimation algorithm which is both *fast* and *adaptive* to time-varying respiration change. For this purpose, Instead of relying on computationally expensive estimation schemes, such as power spectral density (PSD) maximal estimation [23] or peak detection [17], our system applies an extended Kalman filtering (EKF) to directly estimate the signal parameters including the signal frequency from RF measurements.

We implement *RespiRadio* with a pair of laptops equipped with COTS WiFi network interface cards (NIC). We conducted extensive side-by-side experiments to compare *RespiRadio* with two state-of-the-art COTS device based systems, namely WiFi COTS based system (*WiFiBre*) [17] and 802.15.4 system (*sensorBre*) [23]. *RespiRadio* estimates the respiration rate with an overall error of 0.152 breaths per minute (bpm) in dynamic environments, where there exist one or two moving persons. This significantly reduces the detection error compared to *WiFiBre* (2.014 bpm) [17] and *sensorBre* (2.421 bpm) [23]. Further, in comparison to the *WiFiBre* and *sensorBre* systems, our EKF estimator reduces both the estimation time and adaptation time.

II. Related Work

In recent years, RF radios have widely been used in a substantial number of ubiquitous sensing applications, ranging from indoor localization [28], activity recognition [34], privacy leakage [18] to respiration rate monitoring [23], [32]. Existing work on RF based non-contact human respiration rate monitoring systems can be divided into two categories: radar based and COTS device based.

Radar Based: High-capability radar based systems (e.g. Doppler Radar [16], [36], UWB radar [6], [24], [25]) analyze the wireless signals directly affected by movement of the chest cavity to infer the respiration rate. In particular, Doppler radar systems [16], [36] can detect periodic Doppler frequency/phase shift that indicates the respiration rate. UWB radar [6], [24], [25] is leveraged to isolate the signal-path component corresponding to the respiration person. Given that the signals in the respiration-induced path change periodically with a rate identical to the respiration pace, UWB radar based systems infer the respiration rate by analysis of the period of isolated signals on this path accurately and non-intrusively. However, the expensive hardware required for high-capability radar prevents ubiquitous deployment in home settings.

COTS Device Based: Seminal work of COTS based respiration rate monitoring is proposed in [23], where a wireless network composed of 20 IEEE 802.15.4 sensor nodes is deployed to monitor the respiration of a person. Subsequently, the authors improve their monitoring system by implementing novel schemes of channel diversity and oversampling, so that the RSS measurements from a pair of IEEE 802.15.4 TX-RX nodes suffice for respiration monitoring. A COTS RFID based respiration rate monitoring system is proposed in [12], where the RFID tags are requried to attached to users' clothes. With the modified firmware of the Intel 5300 NIC interface, CSI measurements can be acquired, which can be considered as the link quality indicators for 30 independent narrowband subchannels [11]. Hence, as a counterpart to the IEEE 802.15.4 based solution [15], a pair of WiFi devices operated on this modified firmware capable of monitoring a respiration person is demonstrated in [17]. Similar results using Intel 5300 WiFi NIC devices are also introduced in [32], considering different circumstances. Most COTS based respiration monitoring systems are inherently limited by the used RF bandwidth. Therefore, the respiration induced signal path cannot be separately estimated. As a result, those systems may work with stationary environments but perform poorly

in dynamic environments that involve other motions. Besides RF radio signals, Acoustic Signals are also leveraged for respiration detection using the speaker and microphone [33].

III. System Design

RespiRadio has four components, namely power delay profile generation, respiration-induced path isolation, respiration motion detection and respiration rate estimation.

A. Power Delay Profile Generation

Electromagnetic waves propagate roughly in all radial directions. When a radio wave encounters any obstacle, the wave is reflected, resulting in multiple copies of the wave that arrive with a different delay and attenuation at the receiver. This is called the *multipath* effect. The power levels of these multipath signals with increasing delays can be captured by a Power Delay Profile (PDP). Let f be the bandwidth of the radio frequency. We define a *bin* in a power delay profile as *a range of delays*. The *temporal resolution* of a bin for two distinct propagation paths, denoted as t, is determined by the *bandwidth* of the radio frequency f as $t = \frac{1}{f}$ s. The spatial resolution between two distinguishable objects is $c \cdot t$ m , where c is the speed of light. Intuitively, assume that 4 copies of a signal traverse on different paths from TX to RX with propagation delays of 6.2 ns, 18.3 ns, 23.7 ns, and 32.1 ns, respectively, as shown in Figure 1(a). Due to the 20MHz bandwidth limitation, the channel amplitude measurements of the $1st$ bin of the power delay profile are the signal superimpositions of Path $1, 2, 3$ and 4, respectively, as shown in Figure 1(b). In contrast, Figure 1(c) illustrates that all four paths are resolvable when the bandwidth increases to 100 MHz.

For respiration monitoring, only signals on a path reflected from the respiration motion contains relevant information, whereas signal components from all the other paths reflected by other obstacles contaminate the received RF-signals. To verify the importance of RF bandwidth to resilience to motion in a versatile environment, we conduct an experiment, where we ask a subject to randomly walking, while the other stationary subject is concurrently in the region of interest. We capture CSI channel amplitude measurements from the three channels (center frequencies of the three bands are 5.18 GHz, 5.20 GHz and 5.22 GHz respectively, as well each channel band occupies 20 MHz). Figure 2a depict the denoised CSI channel amplitude measurements from three subchannels of the three different channels with 312.5 kHz bandwidth each. We further calculate the respiration rate with the CSI measurements in each subchannel using EKF scheme and achieve an average error of 4.87 bpm. We also generate amplitude of the respiration-person path component from power delay profiles of the synthesized wider-bandwidth WiFi radio using the identical CSI measurements from the three channels shown in Figure 2b. In contrast to the signals in Figure 2a, the amplitude of the signal exhibits better periodicity, which is beneficial for inferring the respiration rate. With these measurements and EKF scheme, the error of respiration rate of the person is reduced to 0.34 bpm, indicating that a wider bandwidth is beneficial to eliminate the impact of the dynamic environments.

Given the limitation of the 88 MHz WLAN clock [19], commercial WiFi cards only support a bandwidth of 20MHz or 40MHz tuned to a specific center channel, covering a non-resolvable temporal delay range of 25 ns or 50 ns (or equivalently, spatial distance range of 7 m or 15 m) in each power delay profile bin. According to the IEEE 802.11 specifications, multiple channels with varying central frequencies are allowed to hop onto, providing an alternative opportunity to acquire a finer-grained power delay profile from a wider bandwidth which has been shown feasible in Splicer [1], [40] and Chronos [30]. However, to synthesize a wider-band radio by synthesizing multiple channels, CSI measurements from these channels must be captured within the *coherence time*, as they are else uncorrelated, and hence invalid for channel synthesis.

For respiration monitoring, the sample rate must be at least 2 times larger than the possible maximal respiration rate due to the Nyquist Theorem. Since a person's typical respiration rate is less than 1Hz [21], our system uses a sampling rate of 2Hz, indicating that the time we utilize to aggregate the CSI measurements for channel synthesis in our system is not allowed to be larger than $T\text{s} = \frac{1}{2\text{Hz}} = 0.5\,\text{s}$. Therefore, to synthesize an RF radio with a spectral bandwidth N times larger than that of a single WiFi channel, the system hops onto N distinct channels to sweep sufficient RF measurements within the 0.5 s.

However, in IEEE 802.11 specifications [2], the reception of a beacon frame by the client (the RX in our system) is used as the indicator that the client is associated with an AP (the TX in our system). Thus, if the AP changes the transmission channel, it loses connection to the client, which is sniffing on the previous channel. In the default IEEE 802.11 protocol [9], the client then re-scans all available channels and then re-associates with the AP after several beacon time intervals. We experimentally verified that this re-association process lasts at least 3 seconds, in which RF-monitoring would be rendered impossible.

To achieve channel-synthesizing within the coherence time, we modify the IEEE 802.11 re-association. Operating on the previous channel, we have the AP broadcast a *channel switch announcement (CSA)* in a specific beacon frame to inform the associated clients that it will switch to a new channel to transmit the next beacon frame, and then automatically switch to the new channel. Once receiving this beacon frame, the client promptly shifts to this channel as well. At the new channel, beacon frames are periodically broadcast by the AP and received by the associated clients; concurrently, data frames are sent to the AP we utilize for respiration monitoring, from which we aggregate the CSI measurements. In this way, channel hopping delay is reduced to 15ms, the theoretical minimum possible in conformance with IEEE 802.11 specifications [2]. Although Chronos [30] boasts 2~3 ms channel switching delay when the AP informs the client with a data frame, this works only in *monitor mode* where clients do not need to associate with an AP to receive its data frames. Monitor mode is, however, not supported by some NIC manufacturers [3], and, more importantly, in general 802.11 networks, most clients are associated with the AP in *managed*

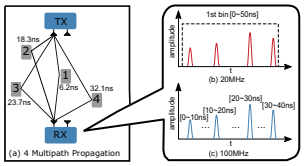

Fig. 1: An example of multipath propagation and corresponding PDPs

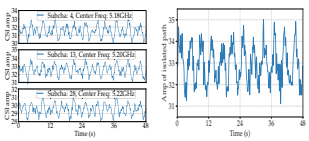

(a) 3 distinct channels **(b)** synthesized radio

Fig. 2: Amplitude of CSI in different sub-channels collected in moving environment

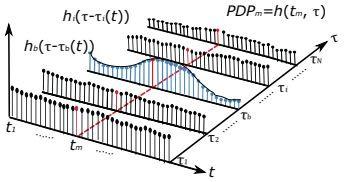

Fig. 3: An example of time-varying multipath PDPs $h(t,\ \tau)$

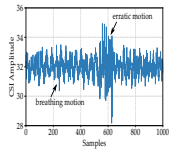

Fig. 4: respiration-path PDPs with both respiration and erratic motion

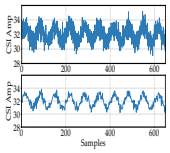

Fig. 5: HMM output performed on measurements shown in Figure 4

mode. Our solution, on the other hand, ensures that all clients associated with the AP switch to the allocated new channel and maintain connection in conformance with IEEE 802.11.

Once our system captures CSI measurements from N bands within $T = 0.5\,\text{s}$, we transform frequency-domain measurements to a time-domain power delay profile [40]. Figure 3 illustrates an exemplary diagram of time-varying power delay profiles, which we termed $h(t,\ \tau)$. Note that $h(t,\ \tau)$ is a function of two time related variables, t and τ. The variable t presents the large-scale power delay profile time, $t \in (mT,\ (m+1)T]$, $(m = 0,\ 1,\ 2,\ ...; T = \frac{1}{2\text{Hz}} = 0.5\,\text{s})$. Within each interval of duration t, we translate the CSI measurements from multiple channels to obtain a power delay profile, as denoted by PDP_m (cf. Figure 3). In contrast, the variable τ denotes small-scale time variation in the range of Ts which represents delays of multipaths for a fixed value t. One may think of τ as being a vernier adjustment of time t in each power delay profile. As the blue and black bars of Figure 3 show, we utilize the notations $h_b(\tau - \tau_b(t))$ and $\sum_i h_i(\tau - \tau_i(t))$ to represent the channel amplitude measurements in the delay bin of time-varying power delay profiles corresponding to a respiration person and the power measurements of all other power delay profile bins at any time t respectively. The multipath power delay profiles can be mathematically expressed as $h(t,\ \tau) = h_b(\tau - \tau_b(t)) + \sum_i h_i(\tau - \tau_i(t))$.

B. Respiration-induced Path Isolation

For respiratory rate estimation, we propose to isolate the power delay profile bin of $h_b(\tau - \tau_b(t))$ from $h(t,\ \tau)$ via signal periodicity. Specifically, other objects are either stationary, causing mostly invariant channel amplitude of these power delay profile bins, or else channel amplitude of the power delay profile bins changes abruptly and randomly due to sudden variations. In both cases, the captured power delay profile bins $h_i(\tau - \tau_i(t))$ from every path not affected by respiration motion does not change periodically with time. Hence, we postulate that only $h_b(\tau - \tau_b(t))$ exhibits periodicity related to the respiratory rate. To reduce the processing overhead of the periodicity detection, one of the first five power delay profile bins is considered as the delay bin of the respiration person. This is a plausible assumption since more than 70% of the energy is transferred via the first Fresnel zone [13]. If the distance between TX, RX and the person is too large, the variation of received power affected by the person's inhaling and exhaling is too weak to recognize over quantization and Gaussian white noise [32].

Our system identifies whether the measurements of any power delay profile bin are periodic or not by comparing the maximal power of measurements in this bin with that of the *permutation* of these measurements. Let φ denote the sequential channel amplitude measurements of any power delay profile bin. In order to examine the periodicity of φ, which can indicate whether φ is $h_b(\tau - \tau_b(t))$ or not, we first conduct a *"scrambling"* process on the measurements to obtain a random *permutation* of φ, termed $\widetilde{\varphi}$. After this process, the measurements $\widetilde{\varphi}$ are random and will not retain the property of periodicity even if the original measurements φ are cyclic. Then, we calculate the maximum power of $\widetilde{\varphi}$ at a frequency band by $p_{\max} = \arg\max_f |\widetilde{\Phi}(f)|^2$, where $\widetilde{\Phi}(f) = FFT(\widetilde{\varphi})$. Given the randomness and disorder of $\widetilde{\varphi}$, the power $|\widetilde{\Phi}(f)|^2$ in every frequency band f tends to be *evenly distributed*. If φ are periodic (in our case, $\varphi = h_b(\tau - \tau_b(t))$), the power of φ is concentrated at its cyclic frequency, f_j so that the power $|\Phi(f_j)|^2$ should be much larger than $p_{\max}$. In the other case, once φ are originated from the other multipaths (in our case, $\varphi = h_i(\tau - \tau_i(t)),\ i \neq b$), at any frequency bin, f_j, the power $|\Phi(f_j)|^2$ should be similar with $p_{\max}$, as both sequences are non-periodic. Hence, we leverage a power threshold p_{thre} to identify the periodicity of φ (we set $p_{\text{thre}} = 3p_{\max}$), that is, if there exists a frequency, f_j, whose power $|\Phi(f_j)|^2$is larger than the threshold p_{thre}, the corresponding power delay profile bin will be considered as the delay bin reflected by the respiration person. Otherwise, we will examine the the periodicity of $(i+1)$-th power delay profile bin.

C. Respiration Motion Detection

1) Two State Classification with HMM: Since the movements of the respiration person are not directly observable, we propose to leverage a two-state HMM to predict the motion performed. The states of the HMM represent respiration-induced chest movement, e.g. *respiration motion (State S_1)* and non-respiration motions, e.g. *erratic motion (State S_2)*. For a given time window within the k-th time interval, containing w power level measurements $\zeta_n(k)$, $n = 1,\ 2,\ ...w$ in the respiration-path PDP bin, the HMM estimates the probability of being in motion state S_i. Given conditional density functions of the observable feature vector $f_{o|S_i}(o_k)$, $i = 1,\ 2$, and the initial state probability $\alpha_j(o_0)$, we derive the probability to be in state i at the k-th time interval as $\alpha_i(o_k) = \left[\sum_{j=1}^{2} \alpha_j(o_{k-1}) \cdot a_{j,i}\right] \cdot f_{o|S_i}(o_k)$. Here, o_k is the observable symbol extracted from $\zeta_n(k)$, $n = 1,\ 2,\ ...w$, $a_{j,i}$. The predicted motion at the k-th time interval is then $\hat{S}(k) = \arg\max_i \alpha_i(o_k)$. We obtained state transition probabilities based on the experimental results as $A = \{a_{i,j}\} =$

$\begin{bmatrix} 0.92 & 0.08 \\ 0.9 & 0.1 \end{bmatrix}$. In addition, we assume the non-respiration indicative state ($\alpha_1(o_0) = 1$, $\alpha_2(o_0) = 0$).

2) Modeling the Conditional Density Distributions: To build an effective two-state HMM, for any time instant k, our monitoring system should further determine the conditional probability density distributions $f_{o|S_i}(o_k)$ with the observable symbol o_k extracted from $\zeta_n(k)$, $n = 1, 2, ...w$. The blocking or damping of signal components by other objects impacts the amplitude of the received RF-signals, and enables recognizing activities, from both time and frequency domain [29], [35], [38].

a) Distribution of Time-domain Feature: In the context of the two-state motions involved in our system, we observe that the signal variation is more significant in the case of erratic motion. Thus, we utilize *deviation of the signal amplitude to the mean amplitude* within a time interval as *a time-domain feature*, which can quantitatively characterize the intensity of signal variations. For a given time window within the k-th time interval which contains w power level measurements in the respiration-path PDP bin, this feature can be calculated as $\beta_k = \frac{\sum_{n=1}^{w}(\zeta_n(k)-\mu_k)}{w}$, where $\zeta_n(k)$ is the n-th power level measurements in the respiration-path PDP bin and $\mu_k = \frac{\sum_{n=1}^{w}\zeta_n(k)}{w}$ is the mean amplitude of all the measurements for the k-th time interval.

Under S_1, due to the inhaling or exhaling, the power level measurements should fluctuate around the mean value μ_k evenly (a.k.a, $\zeta_n(k)$ is either smaller or larger than μ_k with the same probability). Additionally, these measurements can also be affected by noise (e.g., internal thermal Gaussian White noise and quantization bias from wireless device hardware). Thereby, we presumably approximate the distribution of β_k under State S_1 as a Gaussian distribution with mean value 0 and variance σ_1, so that $f_{\beta|S_1}(\beta_k; 0, \sigma_1) = \frac{1}{\sqrt{2\pi\sigma_1^2}}\exp(-\frac{\beta_k^2}{2\sigma_1^2})$.

In State S_2, given that the respiration-path PDP measurements are expected to fluctuate randomly, we model the density function of β_k to satisfy the Gaussian distribution with mean value 0 and variance σ_2, so that $f_{\beta|S_2}(\beta_k;\, 0, \sigma_2) = \frac{1}{\sqrt{2\pi\sigma_2^2}}\exp(-\frac{\beta_k^2}{2\sigma_2^2})$.

To choose the parameters for σ_1 and σ_2, we note that σ_1 is environment-independent, which indicates that only a one-time calibration is necessary. As for σ_2, though it is environment-dependent (e.g. if the respiration person is close to the TX or RX, the fluctuation is larger than that achieved when the person is far away from the devices.), it is certainly much larger than σ_1 in our monitoring system. Rather than training an accurate σ_2 for every environment, we only set the value of σ_2 to 5 times larger than that of σ_1. In this way, our monitoring system does not require a dedicated training phase for each experimental deployment. We conduct experiments with different deployment configurations with the same setting of parameters as described above. The results demonstrate that it is not necessary to adjust σ_1 and σ_2 of the distributions for the different scenarios to improve the performance of the HMM (see Section IV-B4 and Figure 13 for details).

b) Distribution of Frequency-domain Feature: Furthermore, we note that the spectrum energy of respiration motion is concentrated between 0.1 Hz to 1 Hz in frequency domain, whereas erratic motion usually generates energy components in the frequency band over 1 Hz. Motivated by this observation, we utilize spectral energy summation at frequency bands of over 1 Hz as frequency-domain feature, denoted as ξ. To calculate ξ, we adopt 6 levels of discrete wavelet transform (DWT), which calculates a frequency range for different levels with an exponentially reducing granularity. Specifically, if Level 1 DWT represents a frequency range from 64 Hz to 32 Hz, Level 2 DWT corresponds to 32Hz~16Hz .

under S_1, spectral power out of the frequency range of respiration motion only derives from noise, so its value should be close to 0 and gradually decrease with the increment of frequency. On this basis, we assume the conditional density distribution of ξ_k under S_1 to follow exponential distribution $f_{\xi|S_1}(\xi_k; 0, \nu_1) = \nu_1 exp(-\nu_1\xi_k)$, where ν_1 is the rate parameter.

Correspondingly, under S_2, though almost all erratic motions can cause the power in the spectrum band larger than 1 Hz, total energy profiles corresponding to varying erratic activities are drastically different. For example, the spectral energy induced by torso movement is much larger than that caused by arm swing. Due to this issue, we fail to directly model the distribution of total energy ξ_k to satisfy any well-known distribution. Therefore, we model ξ_k to follow the kernel density-based distribution, benefit of which is that it can estimate the density from data without any assumption of the theoretical distribution. In particular, we model the distribution of ξ_k via the Epanechnikov quadratic kernel given by $f_{\xi|S_2}(\xi_k; 0, \nu_2) = \frac{3}{4}\left(1 - \left(\frac{\xi_k}{\xi_k+\xi_b}\right)^2\right)$, where ξ_b is the power of the respiration frequency band in $0 \sim 1$ Hz and $\xi_k + \xi_b$ is the total power. In this way, whatever the erratic motion is, $f_{\xi|S_2}(\xi_k; 0, \nu_2)$ is always close to 1, whereas, for respiration motion, it is close to 0, indicating that the two states are distinguishable.

To integrate both the time-domain feature and frequency-domain feature into a unified density distribution for probability estimation under State S_1 and S_2, since the two features are non-correlated, with each other, we model the density function of the feature vector o_k as $f_{o|S_i}(o_k) = \frac{1}{2}f_{\beta|S_i}(\beta_k; 0, \sigma_i) + \frac{1}{2}f_{\xi|S_i}(\xi_k; 0, \nu_i)$, $i = 1, 2$.

3) Motion State Detection: In order to validate whether the hypothesis of theoretical conditional density distribution for each observable feature is consistent with the corresponding empirical distribution. To this end, we utilize 500 samples for constructing empirical distributions of each observable feature. Further, the empirical distributions are tested against the Gaussian distribution hypothesis using the Kolmogorov-Smirnov test [7], and the returned P-values are 32%, 41% and 28% for density distributions of $\beta|S_1$, $\beta|S_2$ and $\xi|S_1$ respectively, which, as a result, demonstrate that our assumed density distribution passes the Gaussian hypothesis test. Regarding the distribution hypothesis of $\xi|S_2$, we also test its empirical distribution against the theoretical Gaussian distribution as well as other well-known distributions. Based on the tested results, no empirical distribution can fit its assumed theoretical distribution, so that, as mentioned in Section III-C2, the

density function of $\xi|S_2$ cannot be modeled with any well-known distribution.

D. Respiration Rate Estimation

We infer the breath rate with the above extracted time periods of power delay profile data.

1) RF Measurements Denoising: As visible from the blue line in Figure 5, the extracted stream of the channel amplitude measurements, $\zeta_n(k)$, $n = 1, ..., w; k = 1, 2...$, are still noisy, which is mainly due to internal hardware errors of the TX or RX WiFi NIC, such as quantization error and white noise. These errors are introduced when we stitch CSI measurements from multiple bands, and might also originate from signal paths that are mixed in the same delay bin since they have similar delays. Since the typical respiration rate is lower than 1 Hz, a lowpass filter is designed with a stopband frequency at 1 Hz. Particularly, our system leverages finite impulse response (FIR) filter with passband ripple of 0.05 dB and an attenuation of 40 dB at frequencies that exceed the stopband. Let $\widetilde{\zeta_m}$ be the filtered channel amplitude measurements of the respiration-induced power delay profile bin, where $m = w \cdot (k-1) + n$ (cf. Figure 5). We observe that the denoised measurements $\widetilde{\zeta_m}$, represented by the red line, are less volatile than $\zeta_n(k)$.

2) Bayesian Filtering for respiration Estimation: We propose to apply Bayesian filtering to estimate the respiration rate using $\widetilde{\zeta_m}$. Compared to a PSD based scheme, where a history of N previous time-domain measurements are transformed to frequency-domain coefficients via FFT with a computational complexity of $N \log N$, the Bayesian filtering in each step predicts and updates its estimation from a single new measurement only so that the computation overhead is *a constant*. Our approach is therefore attractive for real-time respiration rate monitoring.

As we all know, Bayesian filtering requires to model a *two-space processes* $\widetilde{\zeta_m} = h(\mathrm{x}_m) + v_m$ and $\mathrm{x}_m = f(\mathrm{x}_{m-1}) + u_m$, where x_m is the *state vector* involved in the unknown parameters, $h(\cdot)$ is the *measurement function* and v_m is the measurement noise, $f(\cdot)$ is the *state dynamics function*, ω_m is the process noise. In our system, as the displacement of a person's chest cavity resembles a sinusoidal function of time, we define the *state vector* is x at time instant $m \cdot T_s$ as $\mathrm{x}_m = (\theta_m, \omega_m, A_m, d_m)^T$, where θ_m is the parameter for the sinusoidal function, ω_m is the phase velocity, A_m is the amplitude and d_m is the DC offset. Hence, the *measurement function* for our system can be written in the form of a state vector as $\widetilde{\zeta_m} = A_m \sin(\theta_m) + d_m + v_m$.

To model the *state dynamics function*, we let $\theta_{m+1} = \theta_m + \omega_m \cdot T_s$, and the other parameters w, A and d be constant with time. We further assume that the values of w, A and d are perturbed with one dimensional zero-mean white noise processes, which are described with variables q_w, q_A and q_d. Therefore, the dynamics function for our system can be described in the form of x_m as [27], $\mathrm{x}_m = \begin{pmatrix} 0 & T_s & 0 & 0 \\ 0 & 0 & 0 & 0 \\ 0 & 0 & 0 & 0 \\ 0 & 0 & 0 & 0 \end{pmatrix} \cdot \mathrm{x}_{m-1} + q_{m-1}$, where the distribution of discrete Gaussian white noise process q_{m-1} is referred as $q_{m-1} \sim \mathcal{N}(0, Q_{m-1})$ with the covariance matrix Q_{m-1} given by [26] $Q_{m-1} = \begin{pmatrix} \frac{1}{3}q_w T_s^3 & \frac{1}{2}q_w T_s^2 & 0 & 0 \\ \frac{1}{2}q_w T_s^2 & q_w T_s & 0 & 0 \\ 0 & 0 & q_A T_s & 0 \\ 0 & 0 & 0 & q_d T_s \end{pmatrix}$.

Since the measurement function is *non-linear*, we linearize the measurement function by applying a first-order extended Kalman filtering (EKF) and acquire the Jacobian Matrix by $H_m = \frac{\partial h(\mathrm{x}_m)}{\partial \mathrm{x}_m} = (A_m \cos(\theta_m), 0, \sin(\theta_m), 1)$.

After modeling the two state-space processes and calculating the Jacobians of the nonlinear measurement function, The *EFK equations* are applied for recursively estimating the state space x_m [27].

Eventually, from the predicted sinusoidal parameter $\hat{\theta}$ in state vector $\hat{\mathrm{x}}$ at each iteration, we estimate the respiratory rate of the person by $f_b = \frac{\hat{\theta}_{m+k|m+k-1} - \hat{\theta}_{m|m-1}}{k}$, denoting the average respiration frequency during the time period $t \in (mTs, (m+k)Ts]$.

IV. Experiments

A. Experimental Setup

Our experiments are designed to verify the performance of our respiration monitoring system in a typical domestic home environment as illustrated in Figure 6. We place a TX-RX pair of COTS WiFi cards with a distance of 2 m in between. The pair of WiFi devices we utilize are two Intel Mini PC NUC Kits integrated with the Atheros AR9462 Mini PCI-e WiFi Chipset. Both of the NUC Kits run the Ubuntu 12.04 OS and the modified Ath9k driver, one of which works in AP mode via the revised Hostapd and provides non-disruptive WiFi services to other WiFi clients at the same time.

By running the IEEE 802.11n protocol in our experimental setting, each received packet includes a CSI reading which represents the link quality for each subchannel. In order to obtain the largest possible synthesized-bandwidth, our system operates at 5 GHz where the spectral band is larger than at 2.4 GHz. Due to regulation constraints for channel allocation [4], there exist a maximum of 5 successive adjacent channels, composing a maximum joint bandwidth of 100 MHz. Our system sends a beacon frame to implicitly notify the hopping procedure between TX and RX. A latency of 15 ms is required for channel switch when no packets can be received. To sweep the CSI measurements from all these 5 channels within the sampling period of 0.5 s, we use a timer to ensure the TX to send a beacon frame every 100 ms and another timer of 15 ms to start sending data frames. Our system is designed to transmit 4000 frames per second using UDP sockets. Although UDP cannot ensure the reception of every packet, given the higher frame rate compared to that required by our synthesis algorithm, a power delay profile can always be generated.

During the experiments, a person is sitting in the chair and continuously respiration with a pace controlled with the help of an iPhone metronome App [5]. To confirm the reliability of our monitoring system, various experiments are conducted with different respiratory rate and, for each experiment with a specific respiration frequency. Three individuals are advised to perform respiration with different orientation.

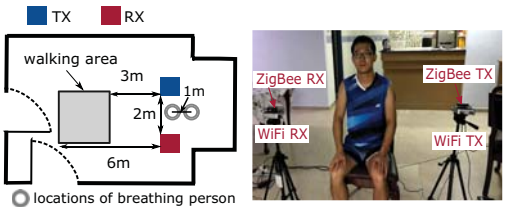

Fig. 6: Floor plan and device deployment of our experimental environment

We evaluate our system with respect to its 1) *accuracy* to isolate the power delay profile delay bin of the respiration person with the synthesized-band RF radio, 2) *precision* to distinguish two different motion-states, 3) *detection accuracy*, *time-efficiency* and *adaptivity* to estimate the respiratory rate in comparison with the conventional PSD scheme and 4) *impact* of TX-RX distance on the respiration detection accuracy. In addition, we compare the performance of our system against two state-of-the-art COTS device based respiration estimation systems, *sensorBre* [15] and *WiFiBre* [17] respectively.

B. Experimental Results

1) Accuracy of Path Isolation: In each deployment scenario, in addition to the person being tested, we advise another person to occasionally enter the test area. The second person is kept at least 3 m apart from the respiration person. Differing from almost all previously proposed COTS device based monitoring systems which are limited by the bandwidth, a key feature of our system is that it is capable of isolating the respiration-induced path component of a power delay profile derived from the synthesized wideband RF signals. Our system does not require the Time-of-Fight (ToF) information in the power delay profile. Instead, our system isolates the signals from the power delay profile delay bin corresponding to the respiration-affected path. We first build a set of groundtruth baselines of respiration-affected paths in the following way. We spatially arrange the chest cavity of the monitored person and the TX-RX pair into a straight line and the first bin of the power delay profile is thus the ground truth of the path from the respiration person. Then, we change the locations of both TX and RX 1.5 m away from the person's chest cavity and the next bin in the power delay profile becomes the ground truth of the respiration-affected path. These distances are chosen since the synthesized-bandwidth of 100 MHz provides a delay resolution of 10 ns, or equivalently, a spatial resolution of 3 m. We repeat the tests until we obtain CSI measurements where the 5-th bin of power delay profile is the ground truth.

A varied number of power delay profile measurements are utilized to identify the respiration-affected path. Hence, we investigate the required number of measurements to correctly identify the path. If the periodicity of the respiration path is confirmed and the isolated path is the same as the baseline path, we say it is correctly isolated. The results are shown in Figure 7. The proposed scheme always correctly identifies the power delay profile delay bin of the respiration-affected path with more than 80 power delay profiles. Also, the results indicate that a higher accuracy is possible with a shorter distance between the respiration person and the TX-RX pair. This is because the larger variation of signals induced by the respiration person can increase the accuracy of detection.

2) Motion State Detection : The motion state of the person being tested is estimated with a HMM as introduced in Section III-C1. We investigate the motion detection accuracy vs. the setting of window duration time and present the results in Figure 8. The results indicate that the two distinct motions are classified with 100% accuracy using a window time of over 3 s.

Additionally, as introduced in Section III-C1, the estimated state transition matrix $A = \{\alpha_{i,j}\}$ should adaptively change in line with periods when the person performs erratic motion during the monitoring process. We calculate the transition probability $\alpha_{i,j}$ by counting the number of S_i and S_j estimated by the HMM respectively and then dividing the number of S_j by the number of S_i and update the state transition matrix A immediately once the latest motion state is estimated with the HMM.

3) EKF vs PSD: Recall that the motivation for our system to estimate respiration rate with EKF has two-fold benefit: 1) it is more time-efficient than PSD and 2) it allows adapting to changes more quickly. Therefore, we compare the performance of EKF with that of PSD in terms of both *computation time* and *time lag*. Firstly, we conduct tests to compare the accuracy as well as computation time for rate estimation with a window length of $N = 10\,\text{s}, 20\,\text{s}, 30\,\text{s}, 40\,\text{s}, 50\,\text{s}, 60\,\text{s}$ and with a fixed baseline respiration rate at 12, 16 and 20 bpm, respectively. As seen from Figure 10 and Figure 11, compared to PSD based respiration detection, the EKF based solution drastically reduces the computation time for respiration estimation while achieving comparative estimation accuracy. The mean absolute error is always less than 1 bpm, which is usually the granularity of the respiration monitoring instrumentation [23]. Even better, with a small window length (e.g., $N = 10\,\text{s}, 20\,\text{s}$), the mean absolute error achieved by the EKF based scheme is much lower than that of PSD, experimentally supporting the conclusion that a larger FFT window length is required for increasing the estimation accuracy.

Since under realistic conditions, a person may change respiration rate, an estimation scheme which can quickly adapt to the change is required. In order to evaluate whether the performance of EKF is better under varying respiration rates, we conduct further tests in which the person increases the respiration rate by 2 bpm each minute from 12 bpm to 20 bpm. We calculate the time latency between the true timing when the person changes respiration rate and the timing when the estimated rate gets close to the ground-truth rate (< 0.5 bpm). The results are depicted in Figure 12. The results validate that PSD is inferior to EKF in adapting to the time-varying change of respiration rate. From the results of Figure 10, 11 and 12, we see that compared with PSD, EKF can strike a better balance in the performance tradeoff in terms of accuracy, time-efficiency as well as adaptability.

4) TX-RX Distance: The detection error achieved at various distances with different fixed respiration rates from 12 bpm to 20 bpm is shown in Figure 9. Additionally, based on experimental results with different respiration rates, our system works effectively up to a range of 9 m. In such a distance, the

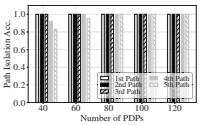

Fig. 7: Number of power delay profiles vs path isolation accuracy

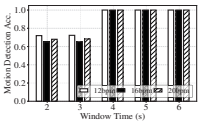

Fig. 8: Window time vs motion detection accuracy

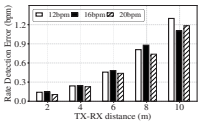

Fig. 9: Distance between TX-RX vs the respiration rate detection error

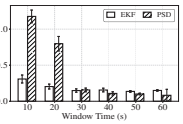

Fig. 10: Respiration rate detection error predicted by EKF and PSD respectively

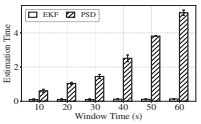

Fig. 11: Estimation time predicted by EKF and PSD respectively

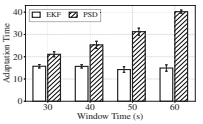

Fig. 12: Adaptation time predicted by EKF and PSD respectively

overall error is still less than 1 bpm.

We conduct another test to validate the statement in Section III-C2 that accurate estimation of the environment-dependent parameter σ_2 is not required to construct the HMM in a varying environment. In several TX-RX distances ranging from $2\,m$ to $8\,m$, we first conduct erratic motion to calculate the accurate value of σ_2, termed as σ_{true}. Then, at the same TX-RX distance, we conduct both respiration motion and erratic motion and then distinguish the two motions using the HMM with the parameters of $\sigma_2 = \sigma_{\text{true}}$ and $\sigma_2 = 5\sigma_1$, which is the default parameter of σ_2 in our system, respectively. Shown in Figure 13, the classification results of the two motions demonstrate that, with both σ_{true} or $5\sigma_1$, the two-state HMM can effectively identify the periods when the respiration person performs erratic motion.

5) Performance comparison: TX-RX COTS based respiration detection systems using WiFi [17] and 802.15.4 [23] have been proposed earlier. We implement both and compare their performance with our system. All three schemes run simultaneously to capture raw RF measurements. As shown in Figure 6, the MEMSIC TelosB ZigBee sensors are placed alongside the NUC toolkit to obtain RSS measurements. With respect to the CSI measurements utilized in the WiFi based system [17], we directly use the same measurements as those obtained for our system. To compare the accuracy of respiration rate detection leveraging the three systems, we conduct two experiments under two different environmental scenarios. Both tests are conducted with different respiration rates at 12, 14, 16, 18 and 20 bpm respectively.

a) Stationary Environment: The first experiment is designed to compare the accuracy of the systems in a stationary ambient environment, which is the presumed condition of the other two systems. It is worth noting that the test allows the respiration person to occasionally change the posture or swing arms/legs since all three systems have demonstrated distinct solutions to detect erratic motion. In the stationary environment, as shown in Figure 14, the accuracy of our system is comparable with the other two system.

b) Disturbed Environment: Commonly, the assumption of stationary environment does not hold. To validate the capability of our system to detect respiration rate in a disturbed environment, the second set of experiments is conducted in more realistic scenarios where the ambient surrounding is continuously changing. In particular, we mimic several practical cases in the monitoring area: 1) a moving person is walking around; 2) two occupants are concurrently present; 3) we repeatedly open or close a door at irregular intervals; 4) a fan works in the monitoring area. From all cases, we conduct experiments with a varying distance between the moving objects and the respiration person ranging from 3 m to 6 m. Figure 14 shows the results of the four tests with the respiration rate ranging from 12 to 20 bpm. In the previous three cases, the mean detection error achieved by our system is significantly lower than that of the other two systems. These results support the assertion that our system is more robust due to its resilience to the dynamics of ambient environment. We also observe that the performance of the other two compared systems deteriorates when the distance between extraneous clutter(s) and respiration person shrinks. This finding can be explained through Fresnel zones. The smaller the Fresnel radius, the smaller the overall attenuation of any movement. Therefore, the disturbed signal component has a larger amplitude when the distance to the respiration person is reduced. Furthermore, as shown in Figure 15d, similar to *WiFiBre* and *SensorBre, RespiRadio* is not influenced by a fan as well, since the periodicity of a fan is much higher than that of an individual which is eliminated by the lowpass filter utilized in our system.

V. Conclusion

In this paper, our key technical contribution is three fold. First, we propose a scheme to synthesize a much wider-bandwidth RF radio with a pair of WiFi devices. Second, with such a synthesized wider-bandwidth RF radio, we introduce several novel schemes, including the breath-induced path isolation, HMM based breathing motion detection and EKF based respiration rate estimation to infer the breathing rate of the monitored person accurately and efficiently in the presence of ambient dynamics. Third, we implemented *RespiRadio* using two COTS WiFi devices and evaluated it in several different scenarios. The experimental results show that *RespiRadio* outperforms two state-of-the-art monitoring systems using COTS devices in terms of time-efficiency, adaptability and robustness to changing environments.

Acknowledgment

This work has been supported by Singapore MOE Tier 2 grant MOE2016-T2-2-023, Tier 1 grant 2017-T1-002-047, NTU CoE grant M4081879, National Science Foundation under Grant Numbers CNS-1837146 and IIP-1632051, and the National Natural Science Foundation of China under Grant Numbers 61872082, 61472184, and the Jiangsu Innovation and Entrepreneurship (Shuangchuang) Program. Jun Zhao's research was supported by Nanyang Technological University (NTU) Startup Grant (M4082311.020), Singapore Ministry of Education Academic Research Fund Tier 1, and Alibaba–NTU Singapore Joint Research Institute.

References

[1] Atheros CSI Tool, http://wands.sg/research/wifi/AtherosCSI/.
[2] IEEE Std. 802.11n-2009: Enhancements for higher throughput.

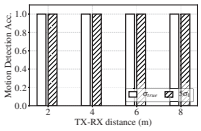

Fig. 13: Motion detection accuracy by HMM with different value of σ_2

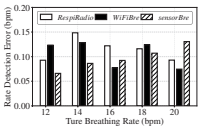

Fig. 14: Error of *RespiRadio* vs *WiFiBre* and *sensorBre* in the stationary environment

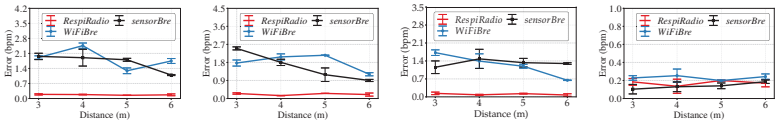

(a) One walking person **(b)** two walking persons **(c)** A door is repeatedly open or closed **(d)** presence of a fan

Fig. 15: Respiration rate detection error of *RespiRadio* vs *WiFiBre* and *SensorBre* in four distinct noisy environments

[3] https://docs.kali.org/installation/troubleshooting-wireless-driver-issues.

[4] http://www.hypercable.fr/images/stories/wirake/24_35__5.4_GHZ_international_rules.pdf.

[5] Pro Metronome, https://itunes.apple.com/nz/app/pro-metronome-tempo-keeping/id477960671?mt=8.

[6] Fadel Adib, Hongzi Mao, Zachary Kabelac, Dina Katabi, and Robert C Miller. Smart homes that monitor breathing and heart rate. In *Proceedings of the 33rd annual ACM conference on human factors in computing systems*, pages 837–846. ACM, 2015.

[7] Wilfrid Joseph Dixon, Frank Jones Massey, et al. *Introduction to statistical analysis*, volume 344. McGraw-Hill New York, 1969.

[8] Niki Fens, Aeilko H Zwinderman, Marc P van der Schee, Selma B de Nijs, Erica Dijkers, Albert C Roldaan, David Cheung, Elisabeth H Bel, and Peter J Sterk. Exhaled breath profiling enables discrimination of chronic obstructive pulmonary disease and asthma. *American journal of respiratory and critical care medicine*, 180(11):1076–1082, 2009.

[9] Matthew Gast. *802.11 wireless networks: the definitive guide*. " O'Reilly Media, Inc.", 2005.

[10] Christian Guilleminault, Rafael Pelayo, Damien Leger, Alex Clerk, and Robert CZ Bocian. Recognition of sleep-disordered breathing in children. *Pediatrics*, 98(5):871–882, 1996.

[11] Daniel Halperin, Wenjun Hu, Anmol Sheth, and David Wetherall. Predictable 802.11 packet delivery from wireless channel measurements. In *ACM SIGCOMM Computer Communication Review*, volume 40, pages 159–170. ACM, 2010.

[12] Y. Hou, Y. Wang, and Y. Zheng. Tagbreathe: Monitor breathing with commodity rfid systems. In *2017 IEEE 37th International Conference on Distributed Computing Systems (ICDCS)*, pages 404–413, June 2017.

[13] Hristo D Hristov. *Fresnal Zones in Wireless Links, Zone Plate Lenses and Antennas*. Artech House, Inc., 2000.

[14] S Javaheri, TJ Parker, JD Liming, WS Corbett, H Nishiyama, L Wexler, and GAl Roselle. Sleep apnea in 81 ambulatory male patients with stable heart failure. *Circulation*, 97(21):2154–2159, 1998.

[15] Ossi Kaltiokallio, Hüseyin Yiğitler, Riku Jäntti, and Neal Patwari. Non-invasive respiration rate monitoring using a single cots tx-rx pair. In *Information Processing in Sensor Networks, IPSN-14 Proceedings of the 13th International Symposium on*, pages 59–69. IEEE, 2014.

[16] Changzhi Li, Jun Ling, Jian Li, and Jenshan Lin. Accurate doppler radar noncontact vital sign detection using the relax algorithm. *IEEE Transactions on Instrumentation and Measurement*, 59(3):687–695, 2010.

[17] Jian Liu, Yan Wang, Yingying Chen, Jie Yang, Xu Chen, and Jerry Cheng. Tracking vital signs during sleep leveraging off-the-shelf wifi. In *Proceedings of the 16th ACM International Symposium on Mobile Ad Hoc Networking and Computing*, pages 267–276. ACM, 2015.

[18] Yang Liu and Zhenjiang Li. aleak: Privacy leakage through context-free wearable side-channel. In *IEEE INFOCOM 2018-IEEE Conference on Computer Communications*, pages 1232–1240. IEEE, 2018.

[19] Alex T Mariakakis, Souvik Sen, Jeongkeun Lee, and Kyu-Han Kim. Sail: Single access point-based indoor localization. In *Proceedings of the 12th annual international conference on Mobile systems, applications, and services*, pages 315–328. ACM, 2014.

[20] Carey R Merritt, H Troy Nagle, and Edward Grant. Textile-based capacitive sensors for respiration monitoring. *IEEE Sensors Journal*, 9(1):71–78, 2009.

[21] John Frederic Murray. *The normal lung: the basis for diagnosis and treatment of pulmonary disease*. WB Saunders Company, 1986.

[22] Mark B Norman, Sally Middleton, Odette Erskine, Peter G Middleton, John R Wheatley, and Colin E Sullivan. Validation of the sonomat: a contactless monitoring system used for the diagnosis of sleep disordered breathing. *Sleep*, 37(9):1477–1487, 2014.

[23] Neal Patwari, Joey Wilson, Sai Ananthanarayanan, Sneha K Kasera, and Dwayne R Westenskow. Monitoring breathing via signal strength in wireless networks. *IEEE Transactions on Mobile Computing*, 13(8):1774–1786, 2014.

[24] Natalia V Rivera, Swaroop Venkatesh, Chris Anderson, and R Michael Buehrer. Multi-target estimation of heart and respiration rates using ultra wideband sensors. In *Signal Processing Conference, 2006 14th European*, pages 1–6. IEEE, 2006.

[25] Jussi Salmi and Andreas F Molisch. Propagation parameter estimation, modeling and measurements for ultrawideband mimo radar. *IEEE Transactions on Antennas and Propagation*, 59(11):4257–4267, 2011.

[26] Simo Sarkka. On unscented kalman filtering for state estimation of continuous-time nonlinear systems. *IEEE Transactions on automatic control*, 52(9):1631–1641, 2007.

[27] Simo Särkkä. *Bayesian filtering and smoothing*, volume 3. Cambridge University Press, 2013.

[28] Shuyu Shi, Stephan Sigg, Lin Chen, and Yusheng Ji. Accurate location tracking from csi-based passive device-free probabilistic fingerprinting. *IEEE Transactions on Vehicular Technology*, 2018.

[29] Stephan Sigg, Markus Scholz, Shuyu Shi, Yusheng Ji, and Michael Beigl. Rf-sensing of activities from non-cooperative subjects in device-free recognition systems using ambient and local signals. *IEEE Transactions on Mobile Computing*, 13(4):907–920, 2014.

[30] Deepak Vasisht, Swarun Kumar, and Dina Katabi. Decimeter-level localization with a single wifi access point. In *NSDI*, pages 165–178, 2016.

[31] Swaroop Venkatesh, Christopher R Anderson, Natalia V Rivera, and R Michael Buehrer. Implementation and analysis of respiration-rate estimation using impulse-based uwb. In *Military Communications Conference, 2005. MILCOM 2005. IEEE*, pages 3314–3320. IEEE, 2005.

[32] Hao Wang, Daqing Zhang, Junyi Ma, Yasha Wang, Yuxiang Wang, Dan Wu, Tao Gu, and Bing Xie. Human respiration detection with commodity wifi devices: do user location and body orientation matter? In *Proceedings of the 2016 ACM International Joint Conference on Pervasive and Ubiquitous Computing*, pages 25–36. ACM, 2016.

[33] Tianben Wang, Daqing Zhang, Yuanqing Zheng, Tao Gu, Xingshe Zhou, and Bernadette Dorizzi. C-fmcw based contactless respiration detection using acoustic signal. *Proc. ACM Interact. Mob. Wearable Ubiquitous Technol.*, 1(4):170:1–170:20, January 2018.

[34] Wei Wang, Alex X Liu, Muhammad Shahzad, Kang Ling, and Sanglu Lu. Understanding and modeling of wifi signal based human activity recognition. In *Proceedings of the 21st annual international conference on mobile computing and networking*, pages 65–76. ACM, 2015.

[35] Wei Wang, Alex X Liu, Muhammad Shahzad, Kang Ling, and Sanglu Lu. Understanding and modeling of wifi signal based human activity recognition. In *Proceedings of the 21st annual international conference on mobile computing and networking*, pages 65–76. ACM, 2015.

[36] James E Whitney II and Latasha Solomon. Respiration rate signal extraction from heart rate. In *Aerospace/Defense Sensing, Simulation, and Controls*, pages 104–112. International Society for Optics and Photonics, 2001.

[37] Frank H Wilhelm, Walton T Roth, and Marvin A Sackner. The lifeshirt: an advanced system for ambulatory measurement of respiratory and cardiac function. *Behavior Modification*, 27(5):671–691, 2003.

[38] Joey Wilson and Neal Patwari. Radio tomographic imaging with wireless networks. *IEEE Transactions on Mobile Computing*, 9(5):621–632, 2010.

[39] Hao-Yu Wu, Michael Rubinstein, Eugene Shih, John Guttag, Frédo Durand, and William Freeman. Eulerian video magnification for revealing subtle changes in the world. 2012.

[40] Yaxiong Xie, Zhenjiang Li, and Mo Li. Precise power delay profiling with commodity wifi. In *Proceedings of the 21st Annual International Conference on Mobile Computing and Networking*, pages 53–64. ACM, 2015.